Global and Planetary Change 67 (2009) 62–77

Contents lists available at ScienceDirect

Global and Planetary Change

journal homepage: www.elsevier.com/locate/gloplacha

A satellite-based Daily Actual Evapotranspiration estimation algorithm over South Florida

Le Jiang [a], Shafiqul Islam [b,*], Wei Guo [a], Antarpreet Singh Jutla [b], Sharika U.S. Senarath [c], Bruce H. Ramsay [d], Elfatih Eltahir [e]

[a] IMSG at NOAA/NESDIS, NOAA Science Center, Camp Springs, Maryland 20746, United States
[b] Department of Civil and Environmental Engineering, Tufts University, Medford, MA, 02155, United States
[c] South Florida Water Management District, West Palm Beach, Florida 33406, United States
[d] NOAA/NESDIS/ORA, NOAA Science Center, Camp Springs, Maryland 20746, United States
[e] Department of Civil and Environmental Engineering, MIT, Cambridge, MA 02139, United States

ARTICLE INFO

Article history:
Accepted 8 February 2008
Available online 3 January 2009

Keywords:
remote sensing
evapotranspiration
AVHRR
Priestley–Taylor
Evaporative Fraction

ABSTRACT

Water resources and agricultural applications require the knowledge of evapotranspiration (*ET*) over a range of spatial and temporal scales. Due to paucity of surface based hydro-meteorological stations, the spatial resolution of *ET* estimates is fairly coarse and is not particularly suitable or reliable for hydrologic modeling, water resources planning and decision making. An *ET* estimation algorithm has been developed by combining data from satellite and ground observations. The method extends the applicability of a commonly used energy balance formulation of *ET* and utilizes the contextual relationship between remotely sensed surface temperature and vegetation index. The required parameters are derived from the Advanced Very High Resolution Radiometer (AVHRR) aboard NOAA-14 satellite. First, the Evaporative Fraction (*EF*) is estimated by utilizing the relationship between a vegetation index and radiometric surface temperature observed from AVHRR for each day. Then spatio-temporal interpolation and filtering techniques are applied to obtain daily *EF* values for cloudy pixels to produce the *EF* map for the entire region. Daily Actual *ET* (*DAET*) maps are derived from these *EF* maps and net radiation maps obtained from ground-based observations. The comparisons between satellite derived *DAET* and ground measurements showed overall low bias and root-mean-square-error for both clear and cloudy days at South Florida in 1998 and 1999. The proposed satellite-based *DAET* (SatDAET) algorithm has its *EF* component primarily estimated from satellite data and the resulting *DAET* has been validated using multi-year ground observations over the South Florida region. The SatDAET algorithm appears to be robust and has the potential to provide near real-time land surface evapotranspiration monitoring over large heterogeneous areas at a very fine spatial and temporal resolution.

1. Introduction

Evapotranspiration (*ET*) is important for water resources management, hydrometeorological predictions, environmental conservation, and agriculture competitiveness. Agriculture alone in the United States accounts for 80% of the nation's consumptive water use. Crop yield decreases if irrigation and rainfall amounts are not equal to *ET*, while excessive irrigation may cause percolation of water along with agri-chemicals below vadoze zone. Accurate and temporally continuous *ET* estimation over large areas will provide valuable assistance to efficient water use and irrigation management.

ET is an indicator of the rate of change of the global water cycle, and is a necessary variable for most numerical weather forecasting and global climate model simulations. Depending on water availability, climate regimes, and landscape conditions, *ET* can represent a substantial portion of the regional water budget. For example, in comparison to the long-term averaged precipitation of 1346 mm (or 53 in.) per year over the South Florida Everglades, the long-term averaged and spatially variable *ET* ranges between 889 mm (or 35 in.) and 1397 mm (or 55 in.) thus representing a substantial portion of the water budget for the ecosystem. At present, due to paucity of surface based hydro-meteorological stations all across the globe, the spatial representation of point *ET* estimates is questionable and is not particularly reliable for spatially distributed hydrometeorological modeling and decision making. Remote sensing provides an economically reliable way to estimate *ET* over large heterogeneous areas. Over the past decades, use of remotely sensed land surface data was largely limited to applications that directly detect surface or near surface features such as snow/ice mapping, vegetation mapping, and cloud masking.

Modeling approaches for point estimation of *ET* perform reasonably well for different sites. For distributed *ET* estimation, however,

* Corresponding author. 113 Anderson Hall, 200 College Ave, Tufts University, Medford, Massachusetts 02155, United States. Tel.: +1 617 627 4290.
E-mail address: Shafiqul.Islam@tufts.edu (S. Islam).

0921-8181/$ – see front matter © 2009 Elsevier B.V. All rights reserved.
doi:10.1016/j.gloplacha.2008.12.008

two major difficulties are: (1) necessity of using surface meteorological observations that are not readily available over large areas, and (2) requirement of a complex land surface model which must be interfaced with remote sensing data. Our proposed methodology is intended to avoid complicated parameterizations that involve heat and momentum resistances to energy transfer for *ET* estimation, and to avoid numerous correction procedures. This methodology is based on commonly used energy balance formulation of *ET* (Priestley and Taylor, 1972) and a contextual relationship between remotely sensed temperature and vegetation index. We use the spatial context (i.e., spatial variation of collocated surface processes) from satellite images to estimate *ET* with minimum number of free parameters. Our recent research efforts have shown that high-resolution (1-km) Daily Actual *ET* (*DAET*) mapping of land surface is feasible with Advanced Very High Resolution Radiometer (AVHRR) data from once a day afternoon overpass of polar-orbiting satellite NOAA-14 (Jiang and Islam, 1999, 2001; Islam et al., 2002; Jiang and Islam, 2003).

Our initial algorithm development and application over heterogeneous domain under clear sky conditions has shown the simplicity of the method without compromising the accuracy in results. Application of *ET* algorithm, for six clear sky days over Southern Great Plains in US in 1997, showed that the overall error in near noon time surface latent heat flux was about 50.5 Wm^{-2} in terms of root mean square error (RMSE) (Jiang and Islam, 2001), which is about 17.6% of the observed mean. Intercomparison of the method to the commonly used aerodynamic resistance energy balance residual method for surface latent heat flux estimation on theoretical basis and real-time performance showed this method requires fewer surface parameters than the traditional approach and can produce comparable or better results (Jiang and Islam, 2003).

The objective of the present study is to explore the applicability of the original Jiang–Islam method to meet the needs of near real-time operational water resources management practice by providing continuous Daily Actual Evapotransipiration (*DAET*) estimation over the South Florida region for years 1998 and 1999, for both clear and cloudy days. We will introduce a spatial–temporal interpolation scheme that is applicable for efficient utilization of remote sensing signals in potentially near real-time operational mapping of *DAET* over a heterogeneous domain. The enhanced comprehensive algorithm — SatDAET — will be discussed in detail. Section 2 describes the original method with its enhancements to provide *DAET* for clear and cloudy days. Section 3 presents the application of SatDAET algorithm for the South Florida Water Management District (SFWMD) domain. Section 4 presents the results of implementing the enhanced algorithm in a continuous fashion over the domain for all days in 1998 and 1999. The considerations on model performance evaluation metrics and validations by available ground-based observation data for both clear and cloudy days of the results are also discussed in this section. Discussion of uncertainty sources and conclusion is presented in Section 5.

2. Methodology

2.1. Basic framework

ET can be estimated by Priestley–Taylor type models as

$$ET = \phi(R_n - G)\frac{\Delta}{\Delta + \gamma} \quad (1)$$

where R_n is the net radiation, G is the soil heat flux, Δ is the slope of saturated vapor pressure at the air temperature, and γ is a psychrometric constant. This equation is applicable for a range of surface conditions where $R_n - G$ is the driving force for *ET*, $(R_n - G)\frac{\Delta}{\Delta+\gamma}$ is the equilibrium *ET*, and ϕ represents a product of Evaporative Fraction (*EF*) and $\frac{\Delta+\gamma}{\Delta}$. It is important to note that in the absence of significant advection and convection, *ET* cannot exceed $R_n - G$, and hence ϕ has a limited range between 0 and $\frac{\Delta+\gamma}{\Delta}$. In the standard application of the Priestley–Taylor method, ϕ is assumed constant (= 1.26), applicable over wet surfaces. We note here that $\frac{\Delta+\gamma}{\Delta}$ varies from −2.6% to −0.7% with an average of about −1.5% for 1 K variation in near surface air temperature T_a (when T_a increases from 10 °C to 40 °C). The variation of $\frac{\Delta+\gamma}{\Delta}$ is larger when T_a is low. A ϕ value of zero corresponds to pixels with no *ET* and $H = R_n - G$ (where H is the sensible heat flux) while a ϕ value of $\frac{\Delta+\gamma}{\Delta}$ corresponds to pixels with maximum *ET* i.e., $ET = R_n - G$. An advantage of using *EF* (which equals $\phi \cdot \frac{\Delta}{\Delta+\gamma}$) or ϕ is that aerodynamic and canopy resistances are not explicitly needed for *ET* estimation. Our attempt is to resolve ϕ value within the remotely sensed triangular or trapezoid space of surface temperature vs. vegetation index (or the so-called *T*–VI) diagram commonly defined by plotting surface temperature against normalized difference vegetation index (*NDVI*) both derived from remote sensing by daytime polar orbiting satellite observations over a heterogeneous domain. Details of interpolation of ϕ value of each remote sensing image pixel within the triangular *T*–VI diagram are described in Jiang and Islam (1999, 2001, 2003).

In our previous studies, we developed and validated the *ET* algorithm, for clear sky days. Application of the algorithm was limited to clear days and instantaneous surface Evaporative Fraction (*EF*) and latent heat flux mapping from afternoon overpass of AVHRR (onboard NOAA-14 satellite) observations for land surface. Although the original method provided a baseline for the efficient use of remote sensing data for instantaneous surface latent heat flux monitoring from space, the two key requirements — "continuous" and "daily" *ET* estimation — motivated us to address key issues related to optimal utilization of one-time-a-day polar-orbiting satellite data for operational land surface *ET* monitoring.

2.2. Applicability of near noon instantaneous EF to represent daily overall EF

Daily average *EF* (defined as the ratio between total latent heat flux and total available energy within a day) estimation is based on near local noon or afternoon instantaneous *EF*, which is critical for *DAET* mapping when daily average or net radiation data are available. Several studies have concluded that the extrapolation of local near noon *EF* for a whole day under clear sky conditions will only incur very small error (Kustas et al., 1994; Hall et al., 1995; Bastiaanssen et al., 1996). From a physical perspective, when surface evapotranspiration is not limited by large scale atmospheric forcing, the partitioning of surface fluxes (which is represented by *EF* or Bowen ratio) during daytime is mainly determined by land surface properties such as soil moisture, vegetation amount, and surface resistances to heat and momentum transfer — most of which are slowly varying variables/parameters during daytime (say 10AM to 5PM local time) as compared to other fast changing variables (such as surface temperature, radiation) that have much stronger diurnal cycles due to radiation and atmospheric forcing. This relative time invariance property during mid-morning to late afternoon for *EF* has been empirically verified by several studies (e.g., Shuttleworth (1991)) and more recently over South Florida (Sumner, 2002, personal communication). Without continuous observation of land surface during daytime hours, which limits the capability of current generation polar-orbiting satellites, it may be the most defensible approach one can take to use the near noon *EF* derived from an instantaneous satellite overpass for the entire daytime. Further, since daytime and night time soil heat fluxes nearly cancel out, and night time surface sensible and latent heat fluxes are also small compared to daytime magnitudes, the *DAET* can be approximated as

$$DAET = EF \cdot R_n \quad (2)$$

where quantities on the right hand side of the above equation represent daily average *EF*, and daily average R_n respectively.

We have realized that other uncertainties may be introduced when applying the above simplification to the domain of this study — SFWMD. In Eq. (1), we have included soil heat flux (G), but not the stored heat changes in the water column (W) which is generally larger than G in the often standing water conditions of South Florida (German, 2000). After analyzing the available data obtained from the ground stations operated by U. S. Geological Survey (USGS), we found that G on average is less than 1.5% of R_n at daily scale. W is also of similar magnitude as G on average compared to the average R_n but its day to day variation is much larger than G. Eq. (2) assumes that G and W are negligible at daily time scale.

Using the visible (VIS), near infrared (NIR) and infrared (IR) bands remote sensing information, which are not capable of penetrating cloud cover, the only feasible way one can take to estimate land surface properties under cloudy conditions is to infer "what the sensor cannot see" from "what the sensor can see" when no other independent sources of observation or modeling data are available. Since cloud is always in motion and has accumulation and dissipation cycles by atmospheric forcing, there is often a significant portion of time for a particular remote sensing image pixel to be clear during daytime though a single instantaneous satellite image may indicate it is cloudy. If cloud cover is of short duration, it is feasible to infer properties of cloudy pixels in VIS and IR bands from clear pixels that have similar surface types. The current generation polar-orbiting satellites which have continuous earth surface observations at half day or 1 day interval are normally sufficient to detect the background land surface types characterized by slow varying parameters such as *NDVI*, surface albedo, and soil wetness.

For fully and partially cloudy days, the surface *ET* processes may be limited by environmental forcing. Extrapolating the *EF* detected at clear pixels becomes more complicated and questionable due to the reduction in short wave radiation under cloudy conditions. For pixels with similar surface properties (e.g., surface type and vegetation class) but under clear and cloudy conditions, the question remains how relevant the *EF* observed (or derived) on the clear pixels within the same class is to the actual *EF* for pixels under cloud cover. There are some compensating effects on cloudy days: a) reduction in the available energy will cause reduction in sensible, latent and soil heat fluxes; and b) reduction in surface temperature will cause decrease in the gradient of surface and air temperature thus reduction of sensible heat flux and soil heat flux. The cloudy condition is somewhat similar to the night-time situation but not to the extent that net radiation is negative (i.e., from surface to atmosphere) since short wave radiation (i.e., visible light) is still significant though through dominantly diffuse radiation (i.e., scattered reflection by atmospheric particles) instead of directly from sun (as under clear sky conditions). On a clear day, early morning or late afternoon *EF* is higher than the mid-day *EF* (e.g., Betts and Hall, 1998). It is arguably true that early morning and late afternoon R_n values are much lower than the mid-day R_n. Since R_n is the major driving force for surface evaporation, for a given site (i.e., which has a fixed set of land surface properties), when it is cloudy (meaning that R_n is reduced comparing to clear sky), it is similar to the early morning or late afternoon conditions for this same site where *EF* is higher compared to the mid-day clear sky condition. We speculate that there will be a small underestimation of *EF* for cloudy pixels by using extrapolation of clear pixels' detected *EF*. However, the impact in *DAET* is likely to be small if a pixel is heavily cloudy for the full daytime (since the net radiation will also be small), and to be small to moderately large if a pixel is only partially cloudy during daytime (since the net radiation could be moderately large).

The major challenge in SatDAET algorithm is posed by the clouds. The current generation GOES has about 1 km resolution in visible channel and about 4 km resolution at thermal infrared channels. It is much further away from the earth surface than AVHRR, e.g., 36,000 km comparing to ~850 km. In addition, GOES does not possess near IR channel that is critical to derive surface vegetation indices such as *NDVI*. Thus AVHRR can provide much spatially refined observations comparing to GOES. The present approach for temporal extrapolation of near noon instantaneous *EF* to represent the daytime averaged value, and the inference of *EF* for cloudy pixels from other clear pixels

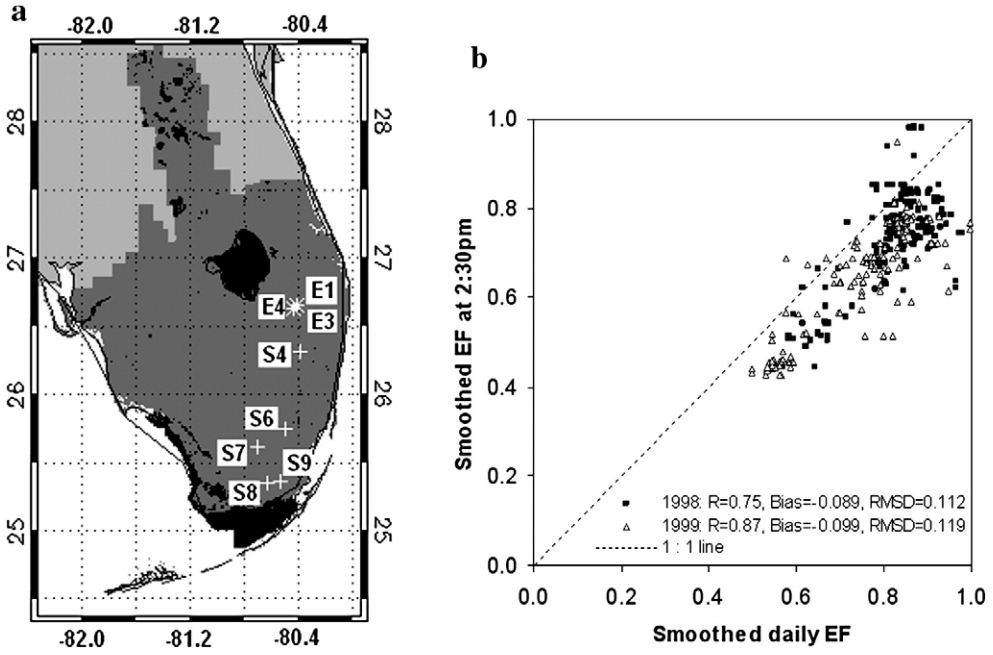

Fig. 1. a). South Florida Water Management District with USGS surface fluxes and *ET* stations (Color scheme for image: white — ocean, light gray — out-of-district area, gray — SFWMD land mass, black — inland water. Station mask symbols: "+" — USGS surface flux stations; "*": *ET* stations. Station name symbols: "S4", "S6", "S7", "S8", and "S9" — USGS surface flux stations 4, 6, 7, 8, and 9; "E1", "E3", and "E4" — *ET* stations ENR104, ENR307 and ENR407). b). Scatter plots of EF_230pm vs. daily *EF* for USGS station S8 in 1998 (black) and 1999 (red). (For interpretation of the references to color in this figure legend, the reader is referred to the web version of this article.)

Table 1
Summary of data availability at USGS stations and actual *ET* measuring stations in 1998 and 1999. Notations in table are explained as following — *ET*: evapotranspiration; R_n: net radiation; d*e*, d*t*: observed gradient of near surface water vapor pressure and air temperature respectively, from which Bowen ratio thus Evaporative Fraction can be derived. The last four columns give the percentage of valid data calculated by the ratio of number of good quality data to the total number of observation intervals in each year for each category.

Year	Station type	Station/landuse	(Lon, lat)	Valid *ET*	Valid R_n	Valid d*e*, d*t*	Valid d*e*, d*t* at 230pm
1998	USGS station	S4/Sawgrass	(−80.3825,26.3153)	90.0%	90.1%	66.1%	76.2%
		S6/Sawgrass	(−80.5031,25.7453)	65.3%	65.3%	64.0%	96.7%
		S7/Sawgrass	(−80.7022,25.6164)	99.7%	99.7%	86.0%	85.2%
		S8/freshwater marsh	(−80.6339,25.3531)	99.9%	100.0%	70.6%	71.0%
		S9/Sawgrass	(−80.5294,25.3597)	95.4%	95.4%	21.3%	26.0%
	ET station in SFWMD	ENR104/sugar cane	(−80.4119,26.6561)	100.0%			
		ENR307/water	(−80.4394,26.6228)	100.0%			
		ENR407/water	(−80.4397,26.6231)	100.0%			
1999	USGS station	S4/Sawgrass	(−80.3825,26.3153)	63.3%	63.4%	51.8%	89.3%
		S7/Sawgrass	(−80.7022,25.6164)	98.8%	98.8%	95.6%	97.0%
		S8/freshwater marsh	(−80.6339,25.3531)	93.7%	96.0%	52.2%	56.7%

with similar surface properties, avoids the use of a complex soil–vegetation–atmosphere-transfer model.

ET in wet areas in South Florida is almost equal or greater than rainfall during dry years (German, 2000). Fig. 1a shows heterogeneous SFWMD landmass that extends from 82.32°W to 79.94°W and 24.37°N to 28.56°N. The major land classes, after excluding water and ocean pixels, are Improved Pastures (approximately 15%), and Urban and Built-Up (approx. 13%). Other significant classes are Sawgrass (approx. 10%), Cypress and Mixed-Cypress (approx. 8%), Citrus Groves (approx. 7%), and Pine Flatwoods (approx. 6%). In our pilot project (Islam et al., 2002), we have investigated the validity of afternoon instantaneous *EF* to represent the daily overall *EF* value for a given site (or pixel in terms of remote sensing) by studying the relationships between daily overall *EF* and afternoon *EF* at about 2:30PM local time for 9 ground-based surface fluxes stations maintained by USGS within the SFWMD domain in 1997 (German, 2000). Summary of location, land use and data availability for operational USGS stations is shown in Table 1.

EF in the afternoon at various sites is close to daily *EF* with very small bias and root-mean-square-error (RMSE). In order to demonstrate, we have plotted the afternoon observed instantaneous *EF* vs. daily *EF* (both quantities are smoothed by a size 3 median filter at USGS surface fluxes stations Site 8 (S8) for 1998 and 1999 inFig. 1b with both clear and cloudy days. The figure suggests that the correlation coefficients are high (to the order of 0.75–0.87), and the bias and RMSE values are low for both years. Given the limited availability of ground-based data and the complexity of spatial and temporal variations of cloud, it appears that the use of afternoon instantaneous *EF* to represent the daily *EF* is reasonable.

2.3. Continuous DAET estimation using space–time interpolation

The spatial and temporal cloud contamination may affect significant portions of total remote sensing images for a particular region within any year. The following section describes SatDAET algorithm in details for the estimation of *DAET* using satellite remote sensing data for all days. Following steps are performed after extracting and mapping the data to a predefined grid from AVHRR channels 1, 2, 4 for VIS, NIR and IR band respectively.

2.3.1. Derive T and NDVI for the region

NDVI is calculated using the channel 1 and 2 reflectance, and surface radiometric temperature, *T*, is calculated using single channel brightness temperature of AVHRR channel 4. The absolute accuracy of land surface temperature (LST) derived from the current generation satellite remote sensing remains to be a challenge given the heterogeneity of land surface. Venturini et al. (2004) concluded that derived *EF* is not very sensitive to the absolute value of remotely derived radiometric surface temperature, but is sensitive to the relative magnitude of temperatures (or temperature difference) among pixels which is relatively easy to detect. Therefore the use of single channel radiometric temperature may be sufficient for the present case. The sensitivity of ϕ to the temperature difference, instead the temperature itself, is evident from the approximate equation for deriving ϕ provided in Section 2.3.3.

2.3.2. Plot T vs. NDVI within the region and determine bounds of the T vs. NDVI trapezoid or triangular space

Previous studies (Carlson et al., 1995, 1997; Jiang and Islam, 1999) have shown that *T* and *NDVI* exhibit a characteristic triangular pattern whose boundaries constitute limiting conditions for the fluxes. After plotting remotely derived *T* vs. *NDVI* for all days in 1998 and 1999, we found that such trapezoid or triangular *T*–VI space exist for almost all days except heavily cloudy days. Fig. 2 shows an example of such a pattern for February 26, 1998 over the SFWMD. In particular, the upper bound of such space can be extrapolated by the warm edge seen on the diagram, and the lower base can be determined using average remotely sensed in-land water body temperature (not under cloud cover). Most of the cloudy pixels are properly identified after this step, which usually fall outside of such bounds. For the lower base, we used a slightly different approach in previous studies such as the lowest observed clear pixel *T* in the image scene (Jiang and Islam, 2001), or $T - T_a = 0$ (Jiang and Islam, 2003). These thresholds are essentially designed to approximate the minimum sensible heat flux (in other words $EF \approx 1.0$ and sensible flux $H \approx 0$) line. In practice, the inland water surface temperature (under clear sky conditions) detected from space is lower than other pixels at daytime and can be used to prescribe such a lower bound. The benefits

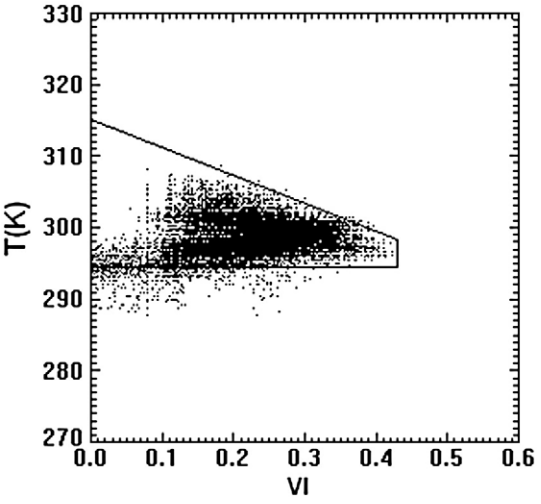

Fig. 2. *T*–VI diagram of February 26, 1998 for SFWMD (solid lines are the bounds for the trapezoidal space).

are two fold: a) inland water bodies are very easy to identify by remote sensing under most cases; b) such treatment eliminates the requirement of near surface air temperature thus increases the practical efficiency of the algorithm and maximizes the use of remote sensing data. We note that remotely derived surface temperature may have large biases due to sun-sensor-target geometry and atmospheric conditions, however, use of remotely derived T may help to cancel out systematic bias because remotely sensed temperature in this algorithm is used in a fashion that only relative magnitude of pixel level T (to the remotely sensed inland water pixel temperature) is important.

2.3.3. Calculate ϕ map using the trapezoid or triangular space for clear pixels

After the bound of T–VI space is determined, we can calculate ϕ value for each pixel within that space by the two-step linear interpolation (Jiang and Islam, 2001), or simply using the following approximate equation

$$\phi \approx \phi_{\max} \frac{T_{\max} - T}{T_{\max} - T_{\min}} \tag{3}$$

where $\phi_{\max} = 1.26$ (Priestley and Taylor, 1972) and T is the remotely sensed surface temperature. $T_{\max}$ and $T_{\min}$ are the maximum and minimum T respectively in the triangular T–VI space. The details of the method are mentioned in Jiang and Islam (1999).

2.3.4. Convert ϕ to EF for clear pixels, leave problematic pixels (i.e., cloud pixels) masked

For pixels which have ϕ values derived in Section 2.3.3 above, we can further convert ϕ to *EF* by

$$EF = \phi \cdot \frac{\Delta}{\Delta + \gamma} \tag{4}$$

where γ is the psychrometric constant (unit hPa/K). Though weakly dependent on near surface air temperature T_a and barometric pressure, γ is often taken as constant for simplicity. The slope of saturated vapor pressure at the air temperature Δ (unit hPa/K) can be calculated as

$$\Delta = \frac{26297.77}{(T_a - 29.65)^2} \cdot \exp\left[\frac{17.67 \cdot (T_a - 273.15)}{T_a - 29.65}\right]. \tag{5}$$

Usually, T_a (K) is one of the most routinely observed variable by meteorological stations. The mean observed air temperature within the domain around satellite overpass time would be sufficient to provide high certainty in Δ given its low sensitivity to T_a. If T_a observation is not conveniently available, remotely sensed mean inland water surface temperature can be used as surrogate without incurring much error.

2.3.5. Fill EF values for cloudy pixels

If there are no clear pixels for the entire remotely sensed image, we leave all values of *EF* for the whole image blank (or masked), but such pixels are assigned an *EF* value by temporal interpolation which is described in Section 2.3.6).

For cloudy pixels (i.e., when the image is partially cloudy), we get an *NDVI* from the previous day (not necessarily yesterday) which is clear and closest in time to the current day.

(1) Case 1: Get an averaged *EF* value within the same *NDVI* of the current image if such *NDVI* exists (within ± 0.01 difference in *NDVI* value) in the current image scene, i.e., there are clear pixels within the current image scene that have the same or very close *NDVI* value to the cloudy pixel.
(2) Case 2: Leave the *EF* value as blank if no similar (or same) *NDVI* values are cloud free in the current image scene. (For an image that is 100% cloudy, all the pixel *EF* values will be left as blank in this step, and the blank *EF* values will be filled by follow-on process described in Section 2.3.6).
(3) The above algorithm will continue pixel-by-pixel for all cloudy pixels until all such pixels are processed.

2.3.6. Temporal interpolation and smoothing

This step consists of the following sequence of processing:

(1) Gap filling — for pixels with no *EF* values, do linear interpolation using *EF* values of neighboring pixels (in time series). After this step, all pixels will have *EF* values.
(2) 5-day median filtering — this will remove extremely high and low values (outliers) of *EF* for a pixel in the time series.
(3) 15-day statistical smoothing, which is intended to get rid of the abrupt changes between days by minimizing the predefined error function.

Such a temporal smoothing technique was suggested by van Dijk et al. (1987) and further improved to produce smoothed weekly global *NDVI* time series by Kogan (1990) to minimize the impacts of clouds.

2.3.7. Calculate daily ET using daily R_n and EF

The final step towards obtaining *DAET* is to apply Eq. (2), where daily R_n map is derived in the current study by spatial interpolation of ground-based measurement from stations in South Florida. The "inverse distance square weighting" spatial interpolation method is used to obtain the R_n map. In our overall SatDAET approach, R_n estimation is independent from *EF* estimation which offers the advantage to assess the uncertainty range for each separately. In this paper, we practically use the spatially interpolated R_n map given that it is not the focus of our current study. It is a limitation and we plan to expand the current algorithm for estimation of *DAET* over heterogeneous areas using a more sophisticated method in which daily net radiation will be estimated from remote sensing. Our recent efforts to develop a remote sensing based net radiation model (Bisht et al., 2005; Batra et al., 2006) which does not require ground-based observations will help to provide better and continuous estimates of *ET* for heterogeneous areas based on primarily satellite remote sensing data.

3. Application of SatDAET algorithm at SFWMD

3.1. Remote sensing data processing

The raw remote sensing data were extracted from the High Resolution Picture Transmission (HRPT) AVHRR data available at the previous NOAA/NESDIS' Satellite Active Archive (SAA) — http://www.saa.noaa.gov, which is now migrated into the NOAA's Comprehensive Large Array-data Stewardship System (CLASS) at http://www.osd.noaa.gov/class. Scanline resolution AVHRR afternoon overpass channels 1, 2, and 4 (i.e., VIS, near IR and IR channels respectively) with associated solar and satellite scan angles information were retrieved from the raw data. Different channels were resampled into the predefined grid that covers the whole South Florida region and has an approximate resolution of 1 km. Such a grid system, called GRID hereafter for convenience, covers 28.56°N, 82.32°W to 24.37°N, 79.94°W and uses the latitude–longitude projection with a resolution of 0.009 degrees. The above rectangle region was represented by a 266-column by 466-row array.

False color images using a composite scheme with red for VIS channel, green for NIR channel, and blue for IR channel were created for each day and saved as reference to visually check the image quality. We then obtained statistics on image quality such as information about cloud amount (using a relatively simple threshold to determine the approximate cloud percentage) and off-nadir angle. The best quality images (e.g., clear days with small off-nadir angles) were

identified. For 1998 and 1999, there are only 4 days with missing data: October 28, 1998, February 11, 1999, February 14, 1999, and September 16, 1999. For these days, both *NDVI* and *T* were assigned invalid value "−1" for every pixel.

3.2. Remote sensing data quality and classification

Clear sky is the desired case for retrieving *ET* from remote sensing data. Unfortunately, about 20% of days in 1998 and less than 10% of days in 1999 are without cloud over the South Florida domain. Cloud amount was approximated primarily by using thresholds of *NDVI*. In the case of South Florida we have used *NDVI* threshold of 0.10 to determine whether a pixel is cloudy or not. High threshold value of *NDVI* is used because of the abundance of vegetation over the domain. It is a very simple treatment to determine cloud amount, however, selection of this threshold was done by trial-and-error with careful visual inspection of multi-channel composite false color images over South Florida for 1998 and 1999.

Scan angle also affects the quality of satellite images and *ET* estimates. The image sections observed at nadir have better resolution and quality than those at off-nadir. For AVHRR, the resolution of the image section at the image edge is normally half of that at nadir. The resolution of the predefined GRID is 0.009°, which equals about 0.896 km at the center of the GRID given the central latitude of the GRID is about 26.5°N (e.g., central resolution is calculated as 6378.137 km*cos (26.5°)*0.009*PI/180 = 0.896 km). The resolution of an AVHRR HRPT image is about 1.0 km at nadir and nearly 2.0 km at the edge of the orbit path, thus it is not surprising that some maps (re-sampled from HRPT data into the GRID) over South Florida are obscure when that region is located at the edge of the scan image with a large off nadir angle.

Images of South Florida were classified based on the cloud amount and off nadir angle. These classified images indicate the days when *ET* can be derived with relatively high certainty. The use of such criteria to select an image only provides an overall view of image quality for a particular day. We recognize that at the pixel scale the clear or cloudy condition is likely to be different than what is indicated for overall image quality.

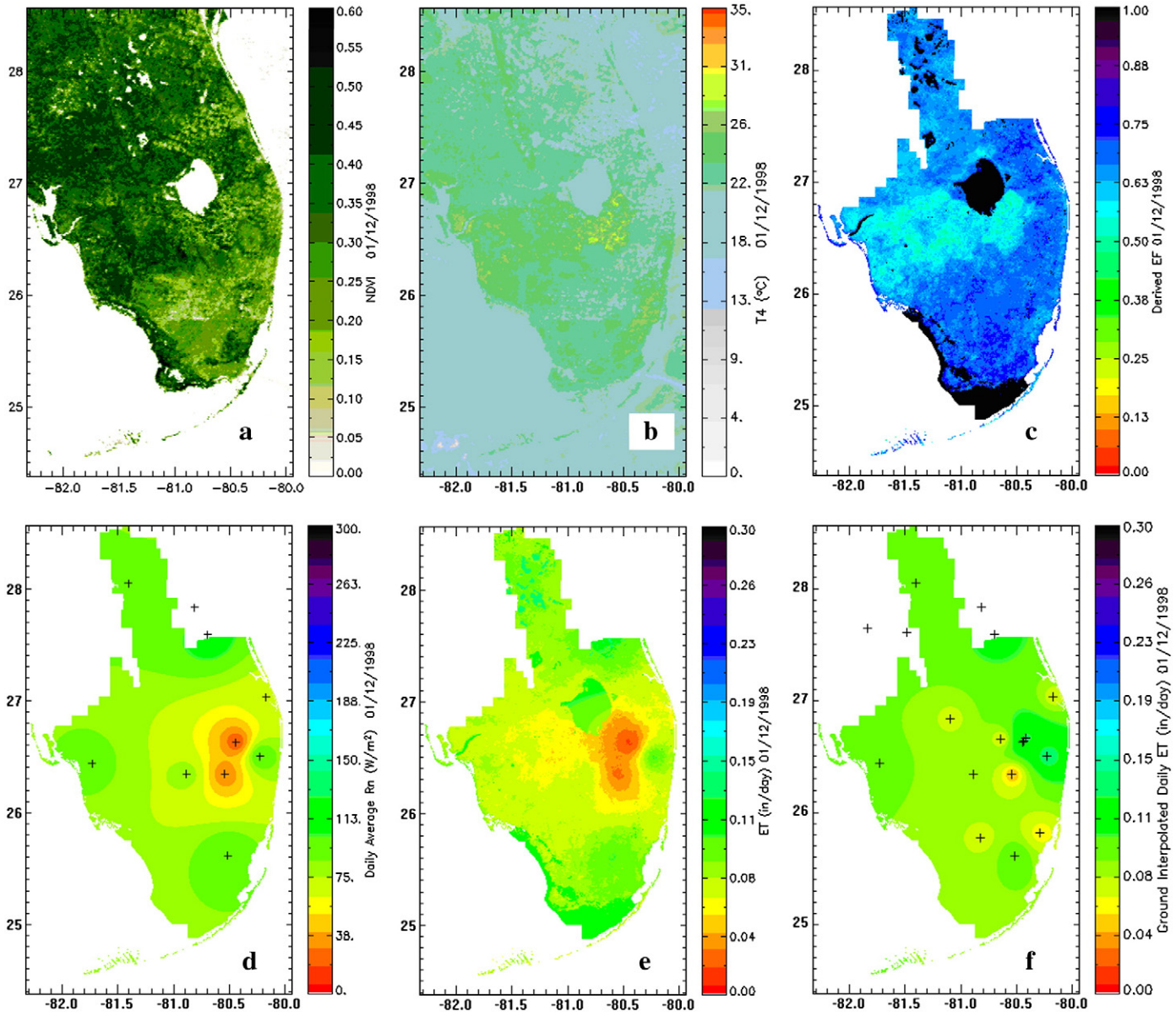

Fig. 3. Maps of a. *NDVI*; b. T4; c. *EF*; d. ground-based R_n; e. satellite derived *DAET*; f. ground-based *DAET* on a clear day January 12, 1998. "+": locations of available ground based stations used for spatial interpolation.

3.3. DAET estimation for 1998 and 1999

For each pixel within the SFWMD region, *NDVI* was calculated using albedos of channels 1 and 2, and *T* was calculated from channel 4. Then, using the algorithm described in Section 2.3, we have derived the *DAET* maps for all 730 days in 1998 and 1999 combined for the SFWMD. This is perhaps one of the first attempts to derive such a large number of high resolution distributed and continuous estimation of *DAET* maps over large heterogeneous areas.

4. Results and validation

4.1. Results of DAET maps for clear and cloudy days

Panel Figs. 3–6 show the *DAET* maps derived using the SatDAET algorithm for clear (Fig. 3), partially cloudy (Fig. 4), cloudy (Fig. 5), and poor image quality (almost overcast) (Fig. 6) days. Note that data points shown on sub-figures of Fig. 3 (a and f) through Fig. 6 (a and f) include additional R_n stations and pan evaporation stations used to obtain ground-based R_n and ground based *DAET* maps. These stations are not included in Fig. 1 or Table 1 which only has the stations used for results validation. The horizontal axes for these plots start from 82.32°W and vertical axes start from 24.37°N. Presented in each panel are remote sensing data derived *NDVI* (Figs. 3a, 4a, 5a, 6a) and *T* (Figs. 3b, 4b, 5b, 6b) maps, from which the image quality (e.g., cloud amount) can be seen, and *EF* (Figs. 3c, 4c, 5c, 6c). Ground data interpolated R_n maps are shown as Figs. 3d, 4d, 5d and 6d. Ground data appears to be much smoother than observed remote sensing data and the derived images due to the small number of available ground stations and the spatial interpolation method (i.e., inverse distance square weighting method) used. For these examples with varying image quality and cloud conditions, our proposed continuous spatial–temporal interpolation scheme (see Section 2.3) has been proved to be effective and has produced *EF* maps with reasonable heterogeneity for the entire SFWMD domain. Figs. 3e, 4e, 5e, and 6e show the resulting *DAET* maps from the production of ground-based R_n maps and satellite derived *EF* maps. These *DAET* maps resemble somewhat the heterogeneity in the *EF* maps and have obvious high (low) value centers reflecting extremely high (low) R_n values seen from the R_n maps. Ground data derived *DAET* maps for visual comparison, are created from spatial interpolation of available ground-based stations are presented in Figs. 3f,

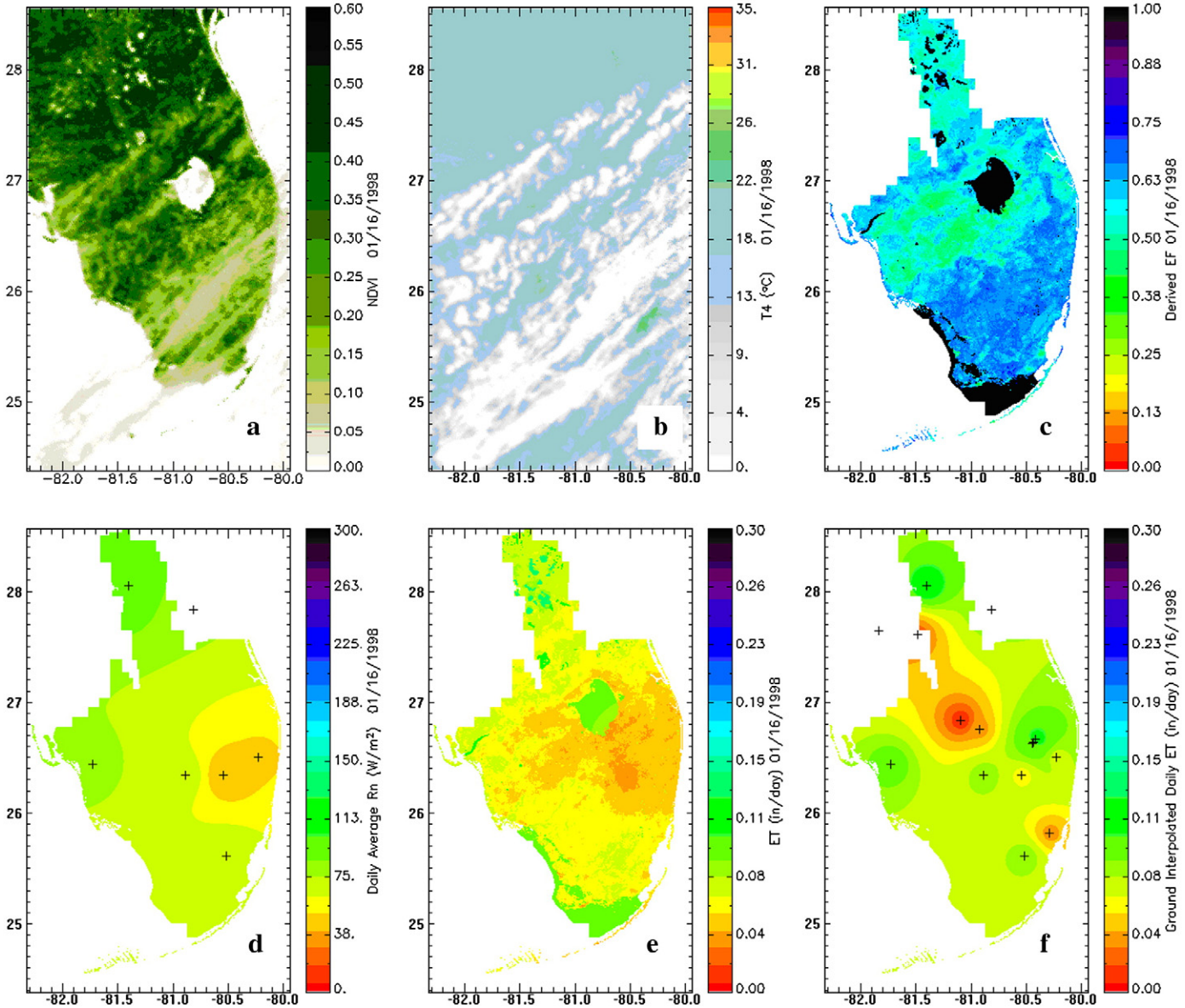

Fig. 4. Maps for a. *NDVI*; b. T4; c. *EF*; d. ground-based R_n; e. *DAET*; f. ground-based *DAET*, on a partly cloudy day January 16, 1998. "+": locations of available ground-based stations used for spatial interpolation.

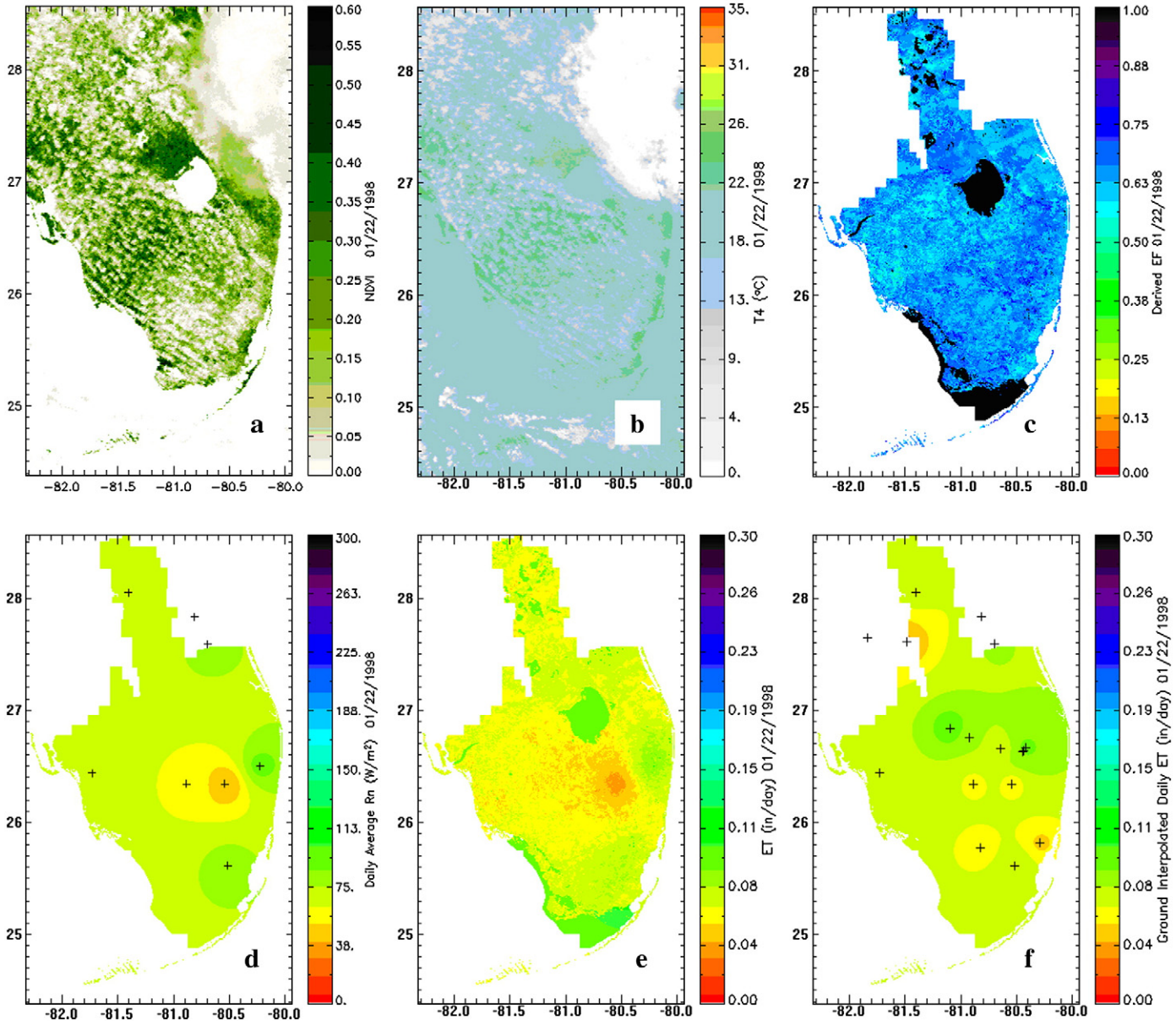

Fig. 5. Maps for a. *NDVI*; b. T4; c. *EF*; d. ground-based R_n; e. *DAET*; f. ground-based *DAET*, on a cloudy day January 22, 1998. "+": locations of available ground-based stations used for spatial interpolation.

4f, 5f and 6f, which showed much spatially smoother patterns than those of remote sensing derived *DAET* maps.

4.2. Ground-based data for validation

The available operational ground stations during 1998 and 1999 were used as an independent data source for validation of *ET* estimates from SatDAET algorithm. Table 1 provides a brief summary of the data availability (relevant to directly obtaining or indirectly deriving *ET*) in 1998 and 1999 for different types of stations.

a). USGS surface fluxes stations

There were 9 surface fluxes stations maintained by USGS with hourly cumulative *ET* and other surface observations in 1997 (for details see German (2000)) within the SFWMD domain shown in Fig. 1a. However, in the 2 years that followed, the number of operational stations, each denoted as "Sn", where *n* represents the station number, were reduced to 5 (i.e., S4, S6, S7, S8, S9) in 1998, and further reduced to 3 (i.e., S4, S7, S8) in 1999 (refer to Fig. 1a for locations of these stations). The stations alone are not adequate to derive a reliable map of ground-based surface *DAET* for the whole area. The dataset appears to be a good candidate for validation purposes. The details of data collection and availability are in German (2000). At each station, the daily *EF* observation time series were smoothed by a size 3 (i.e., 3-day) temporal median filter to remove part of the abrupt changes between consecutive days.

b). *ET* stations

There are several additional *ET* stations located within the GRID for 1998 and 1999 (Fig. 1a). These stations measure or estimate the daily sum of *ET* (in millimeters), or daily sum of potential *ET* (in inches). *ET* estimates at stations ENR104, ENR307 and ENR407 have been obtained using lysimeters. Model estimates (from SFWMD) have also been used to patch these time-series whenever equipment malfunctioned at these stations.

These stations were located in proximity to one another as shown in Fig. 1a, actually within a distance of 5 pixels. We note that *ET* stations ENR307 and ENR407 were co-located at the same map grid, however the

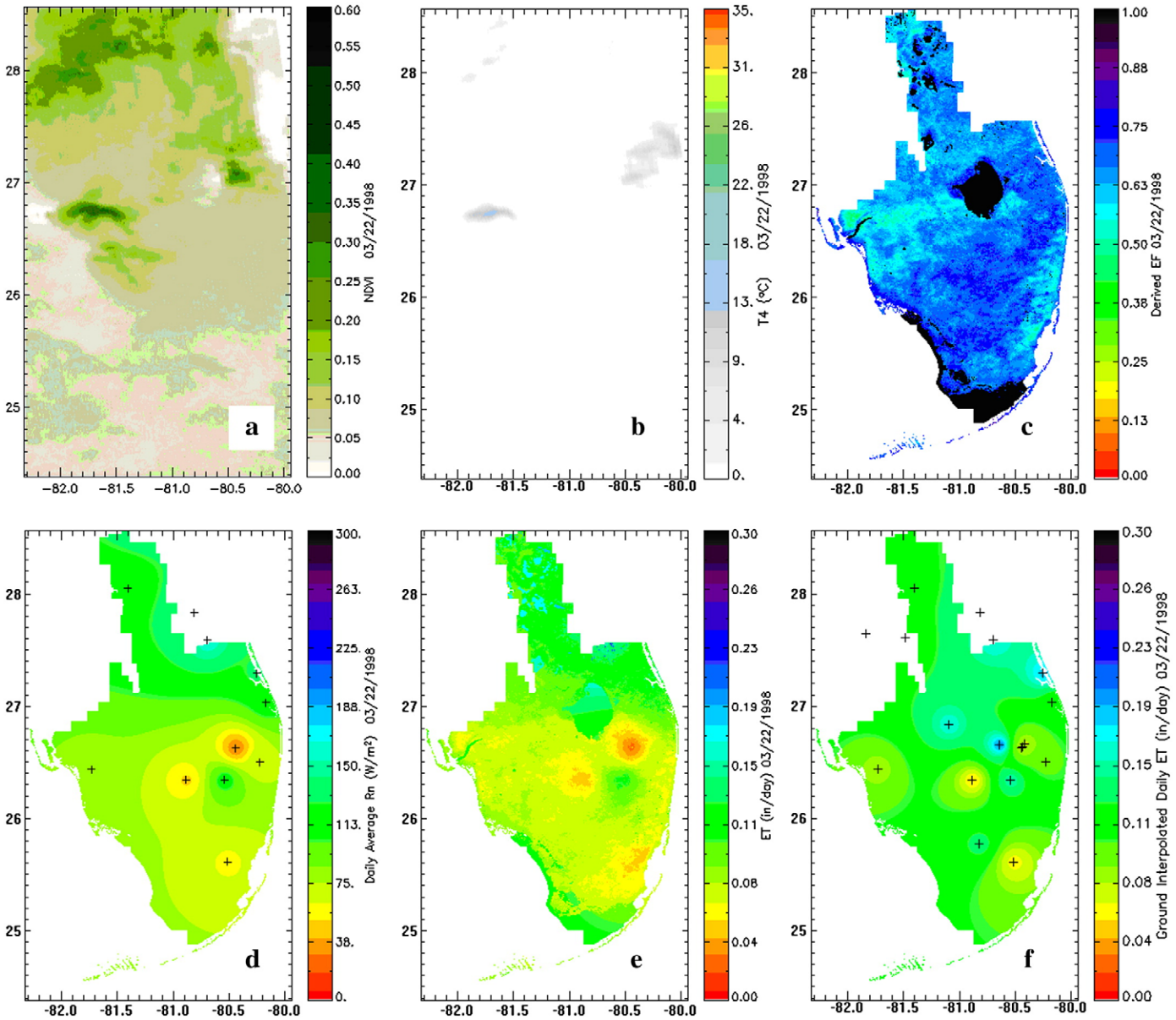

Fig. 6. Maps for a. *NDVI*; b. T4; c. *EF*; d. ground-based R_n; e. *DAET*; f. ground-based *DAET*, on an overcast day (poor image quality) March 22, 1998. "+": locations of available ground-based stations used for spatial interpolation.

annual mean value of *ET* at ENR307 (approx. 4.068 mm/day) is higher than that of ENR407 (approx. 3.758 mm/day), and *ET* at ENR407 appears to have a stronger seasonal trend (Not shown). Such sub-grid heterogeneity in *ET* (e.g., two stations within a distance of approximately 1 km), which is probably caused by the ambient environmental conditions around these stations, highlights the complexity of our task of ground-based validation. The scatter plot analysis of *ET* at ENR407 vs. *ET* at ENR307 suggests that the bias (i.e., mean *ET* at ENR407 minus mean *ET* at ENR307) is −0.310 mm (which is about 7.6% of the observed mean *ET* at ENR307), RMSD (root mean square difference) is 0.844 mm (which is about 20.7% of the observed mean *ET* at ENR307), and correlation coefficient (R) is 0.903. Consequently, we have to be cautious when comparing remotely sensed estimates with ground-based observations.

c). Pan evaporation stations.

Our investigation showed that evaporation time series measured at existing pan evaporation stations are noisier than the *ET* time series at *ET* stations. The annual mean values of pan evaporation time series at different stations appear to be consistently larger than *ET* or potential *ET* stations, which is expected (See Singh (1988) for physical reasons).

We will not validate our *DAET* results against pan evaporation measured *ET*. However, to use pan evaporation stations equivalently with *ET* and potential *ET* stations for the purpose of ground-based spatial *ET* maps interpolation used for comparison, we multiply the observed daily pan evaporation by a commonly accepted pan coefficient of 0.70 (Bras, 1990). Combining the datasets from a) and b) above, the annual mean value of *ET* from USGS stations and SFWMD *ET* stations is about 3.916 mm/day and 3.047 mm/day for 1998 and 1999 respectively.

4.3. Ground based DAET map estimation without remote sensing

Ground based *DAET* maps would help in gaining base line knowledge of the capability of not only a ground-based observation network, but also other modeling approaches that tune model outputs to optimally match ground-based observations. To obtain ground-

based *DAET* maps, we have used the following observed or derived data and considered "non-water" and "water" pixels separately.

i). *ET* estimation for "non-water" pixels.

We have used:

(1) USGS stations that have 30-min observation intervals, and from which daily *EF*, and daily *ET* can be derived;
(2) *ET* stations that have daily *ET* observations;
(3) "Non-water" R_n stations that have daily R_n observations.

For these stations, we derived a spatially interpolated daily *EF* map using USGS stations. Consequently, pixels where R_n stations are located will have daily *EF* values. This was done through an "inverse distance square weighting" approach where daily *EF* value at each R_n station was derived using the weighting function which considers all observed daily *EF* and their distances to the R_n station. Then we calculated *DAET* at each R_n station using $DAET = R_n \cdot EF$. We can now derive a spatial interpolated daily *ET* map for all "non-water" pixels with *ET* observation stations, *ET* from USGS stations, and *ET* from R_n stations derived above.

ii). *ET* estimation for "water" pixels.

We have used

(1) Pan evaporation stations (only those near well watered surfaces were used with a multiplying factor of 0.70).
(2) R_n stations in water pixels that have daily R_n observations.

For these pixels, we used a maximum value of $EF = \phi\Delta/(\Delta+\gamma)$, where ϕ is assumed to be 1.26, and Δ is calculated by Eq. (5) using the afternoon (e.g., near 2:30PM) SFWMD domain averaged T_a observations for this calculation. Then we used an arithmetic average of these *ET* values for a given day as the estimated *ET* for all "water" pixels.

Steps i) and ii) provide ground-based *DAET* for all pixels for each day. We emphasize, however, that the ground-based observation stations are very limited to obtain a realistic and reliable surface *ET* map for each day in 1998 and 1999. Different modeling studies suggest that, depending on the degree of spatial heterogeneity, 5% to 12% spatially distributed point-based observation values are needed to get a reasonably good spatial interpolation (Kitanidis, 1997). Given the extreme paucity of the available ground-based stations (e.g., about 10–15 ground-based stations over an approximately 266 km × 466 km domain represents only 0.012% of the whole region; if we exclude all ocean and out-of-district pixels, we have approximately 0.03% observation pixels). Thus we do not anticipate superior performance of any spatial interpolation scheme to provide a highly reliable spatial map of *ET*.

We have also investigated the mean and standard deviation of time series of ground-based *ET* maps for 1998 and 1999. The annual mean *DAET* for all maps is 3.226 mm/day and 3.023 mm/day in 1998 and 1999 respectively, while the standard deviations for the 2 years is 0.174 mm/day and 0.177 mm/day. These results are in general agreement with the annual trend indicated in Section 4.2 from ground-based stations.

4.4. Validation of SatDAET products using ground-based observations

4.4.1. Consideration of performance evaluation metrics

Willmott (1982) provided an insightful discussion on the use of model performance evaluation metrics especially regarding the use of correlation measures such as correlation coefficient (R or R^2) and difference measures such as bias, root-mean-square-error (RMSE), etc. In particular, it is worthwhile to emphasize the following points made by Willmott (1982) and the references therein. a) Accuracy is defined as the degree to which model-estimated observations approach the magnitudes of their observed counterparts. b) The magnitudes of correlation coefficients (R and R^2) are not consistently related to the accuracy of prediction. For instance, it was demonstrated that correlations between very dissimilar model-predicted variables and observations can easily approach 1.0, while a number of other comparisons illustrate that R and R^2 are insufficient to make meaningful distinctions between models. c) Willmott and Wicks (1980) observed that "high" or statistically significant values of R and R^2 may in fact be misleading, as they are often unrelated to the sizes of the differences between observed and predicted values. It is also quite possible for "small" differences between observed and predicted values to occur with low or even negative values of R. Further, they pointed out since the relationships between R and R^2 and model performance are not well-defined, and not consistent, R and R^2 should not be part of an array of model performance measures.

Therefore in our study, we considered a set of statistics in addition to the correlation coefficient (R) regarding the observed and estimated series. We report the difference measures such as correlation coefficient, Bias, RMSE, the relative different measures $Bias/Mean_{obs}$, $RMSE/Mean_{obs}$, along with the mean, standard deviation, and coefficient of variation (defined as the samples' standard deviation divided by

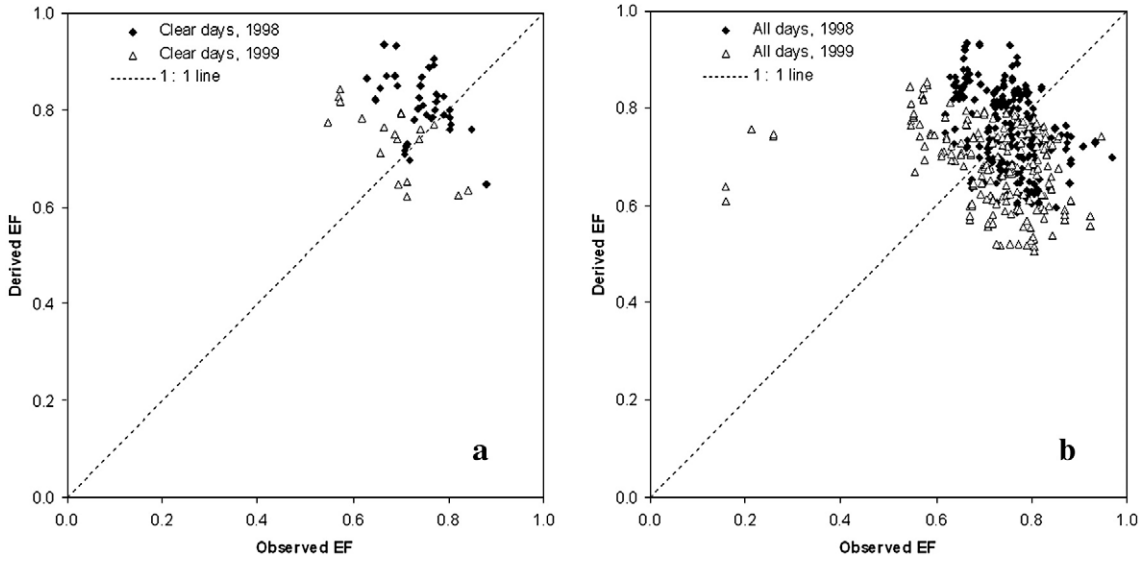

Fig. 7. Comparison of derived *EF* and observed *EF* at S4 for a) most clear days, and b) all days in 1998 and 1999.

Table 2
Summary statistics of observed and estimated *EF* at USGS stations for clear days. The metrics include observed mean ($Mean_{obs}$), observed standard deviation (STD_{obs}), observed coefficient of variation (CV_{obs}), estimated or derived mean ($Mean_{est}$), estimated standard deviation (STD_{est}), estimated coefficient of variation (CV_{est}), Bias, RMSE, correlation coefficient (R), relative error by Bias/$Mean_{obs}$, and relative error by RMSE/$Mean_{obs}$.

Year	Station	$Mean_{obs}$	STD_{obs}	CV_{obs}	$Mean_{est}$	STD_{est}	CV_{est}	Bias	RMSE	R	Bias/$Mean_{obs}$	RMSE/$Mean_{obs}$
1998	S4	0.742	0.057	7.7%	0.810	0.064	7.95%	0.068	0.121	−0.381	9.1%	16.3%
	S6	0.637	0.068	10.7%	0.790	0.095	12.0%	0.154	0.201	−0.292	24.1%	31.6%
	S7	0.724	0.073	10.0%	0.778	0.090	11.6%	0.054	0.152	−0.532	7.5%	20.9%
	S8	0.798	0.101	12.6%	0.781	0.048	6.1%	−0.017	0.122	−0.264	−2.1%	15.2%
	S9	0.732	0.097	13.2%	0.693	0.068	9.9%	−0.038	0.119	0.037	−5.2%	16.3%
1999	S4	0.686	0.080	11.7%	0.739	0.069	9.3%	0.053	0.143	−0.678	7.7%	20.8%
	S7	0.707	0.095	13.4%	0.746	0.098	13.1%	0.039	0.160	−0.332	5.5%	22.6%
	S8	0.682	0.153	22.5%	0.758	0.092	12.2%	0.076	0.242	−0.868	11.2%	35.4%
Mean		0.714	0.091	12.7%	0.762	0.078	10.3%	0.049	0.158	−0.414	7.2%	22.4%

samples' mean) of both observed and estimated (modeled) values to give a comprehensive view of the comparison. We must emphasize, however, correlation coefficient should not be used as a sole metric to compare model performance.

To assess the performance of the algorithm in deriving *EF* and *DAET*, we will validate the estimated quantities separately using ground observed or derived data. In addition, we anticipate the algorithm performance will provide varying degrees of certainty for clear and cloudy days. An important aspect for the validation is to give an assessment of the algorithm's performance a) for clear days only and b) for all days to understand the best case scenario (i.e., clear days) as well as overall capability of the approach.

4.4.2. Validation of satellite derived EF

4.4.2.1. Validation of EF for most clear days. We have selected the most clear days using thresholds of cloud percentage <14% and off nadir angle <40° even though some of the mostly clear days are in fact partly cloudy by visual inspection. This is a coarse classification since the "crystal clear" conditions are rare in each year's annual daily image series. The above selection of thresholds gives a considerably large number of days that are useful to address the realistic capability of the algorithm. The valid observation data percentage varies from 21% to 96% depending on the operational period of performance at each station (See Table 1). As an example, Fig. 7 shows the comparison of derived *EF* and the observed *EF* at the USGS station S4 in 1998 and 1999. We observe that the ground observed *EF*s time series at individual site are relatively stable (probably due to the fact that these stations are installed on relatively wet surfaces) with small variation. We note that the cluster of points in each scatter plot accurately depicts the observed daily *EF* with such clusters located at the upper-right corner of the scatter plots. With the distribution of scattered points shown in Fig. 7a, we anticipate to see low correlation coefficient while on the other hand low bias and RMSE should also be anticipated.

Table 2 gives a summary of a comprehensive metrics at the existing USGS stations. It can be observed that these stations have large *EF* with individual mean of station observed *EF* under clear days ranging from approximately 0.637 to 0.798, and the overall mean about 0.714. On average, the standard deviation of observed *EF* is small, which is about 12.7% (indicated by the mean coefficient of variation for observed series — CV_{obs}) of the observed mean. The estimated *EF* for these stations has similar mean, standard deviation and CV as the observed quantities. The average CV is 10.3%. The average bias is 0.049 and average RMSE is 0.158, which are about 7.2% and 22.4% of the observed mean respectively. The correlation coefficient (R) is small or negative, however, as we anticipated above by examining the scatter plots, small or negative correlation coefficient itself does not necessarily mean poor estimation performance. It is important to look at the comprehensive set of comparison metrics to conclude meaningfully, especially at the difference measures (Bias and RMSE) and relative different measures (Bias/$Mean_{obs}$ and RMSE/$Mean_{obs}$) which are better evaluators of model performance. The lack of variation in the ground-based *EF* time series itself at a particular location may attribute to the low correlation coefficient. However, this should not necessarily lead to the conclusion that using a fixed number for *EF* rather than deriving it from remote sensing would produce a better or comparable result. For the particular site, it is seemingly applicable to use a simple, constant value for *EF* rather than that from the satellite-based method to achieve a good match between estimation and observations under the circumstance that in fact *EF* be fairly constant during a year, but this treatment may lose the generality since it is obviously not in agreement with most field experiment findings especially over regions with clear seasonality. *EF* (which is an indicator of the partitioning of land surface latent and sensible heat fluxes) is generally not a constant, neither spatially (as it is affected by land surface heterogeneity) nor temporarily (as it has day-to-day to seasonal scale variations) (e.g., Betts and Hall, 1998). We further noticed that the observed *EF* values primarily come from one land use class (S4, S6, S7 and S9 belong to saw grass while S8 is freshwater marsh) and have a very limited range. A more robust validation of our satellite-based *EF* would be to compare estimated *EF* values for a wide spectrum of land surface conditions.

In the comparison results shown above, it is clear that our algorithm adequately reproduced the observed daily *EF* within a small error range. The basic algorithm estimates the afternoon instantaneous *EF* which is

Table 3
Summary statistics of observed and estimated *EF* at USGS stations for all days.

Year	Station	$Mean_{obs}$	STD_{obs}	CV_{obs}	$Mean_{est}$	STD_{est}	CV_{est}	Bias	RMSE	R	Bias/$Mean_{obs}$	RMSE/$Mean_{obs}$
1998	S4	0.753	0.064	8.5%	0.755	0.082	10.9%	0/002	0.123	−0.401	0.2%	16.3%
	S6	0.652	0.079	12.2%	0.745	0.097	13.1%	0.094	0.172	−0.332	14.4%	26.4%
	S7	0.744	0.078	10.5%	0.740	0.077	10.4%	−0.003	0.123	−0.273	−0.5%	16.6%
	S8	0.816	0.088	10.8%	0.730	0.078	10.7%	−0.086	0.161	−0.356	−10.6%	19.8%
	S9	0.749	0.101	13.5%	0.673	0.070	10.3%	−0.076	0.159	−0.333	−10.1%	21.2%
1999	S4	0.717	0.123	17.2%	0.687	0.082	12.0%	−0.030	0.171	−0.328	−4.2%	23.9%
	S7	0.743	0.117	15.8%	0.702	0.092	13.1%	−0.041	0.181	−0.409	−5.5%	24.2%
	S8	0.738	0.129	17.4%	0.678	0.104	15.1%	−0.051	0.216	−0.649	−6.9%	29.3%
Mean		0.739	0.097	13.2%	0.714	0.085	12.0%	−0.028	0.163	−0.385	−2.9%	22.2%

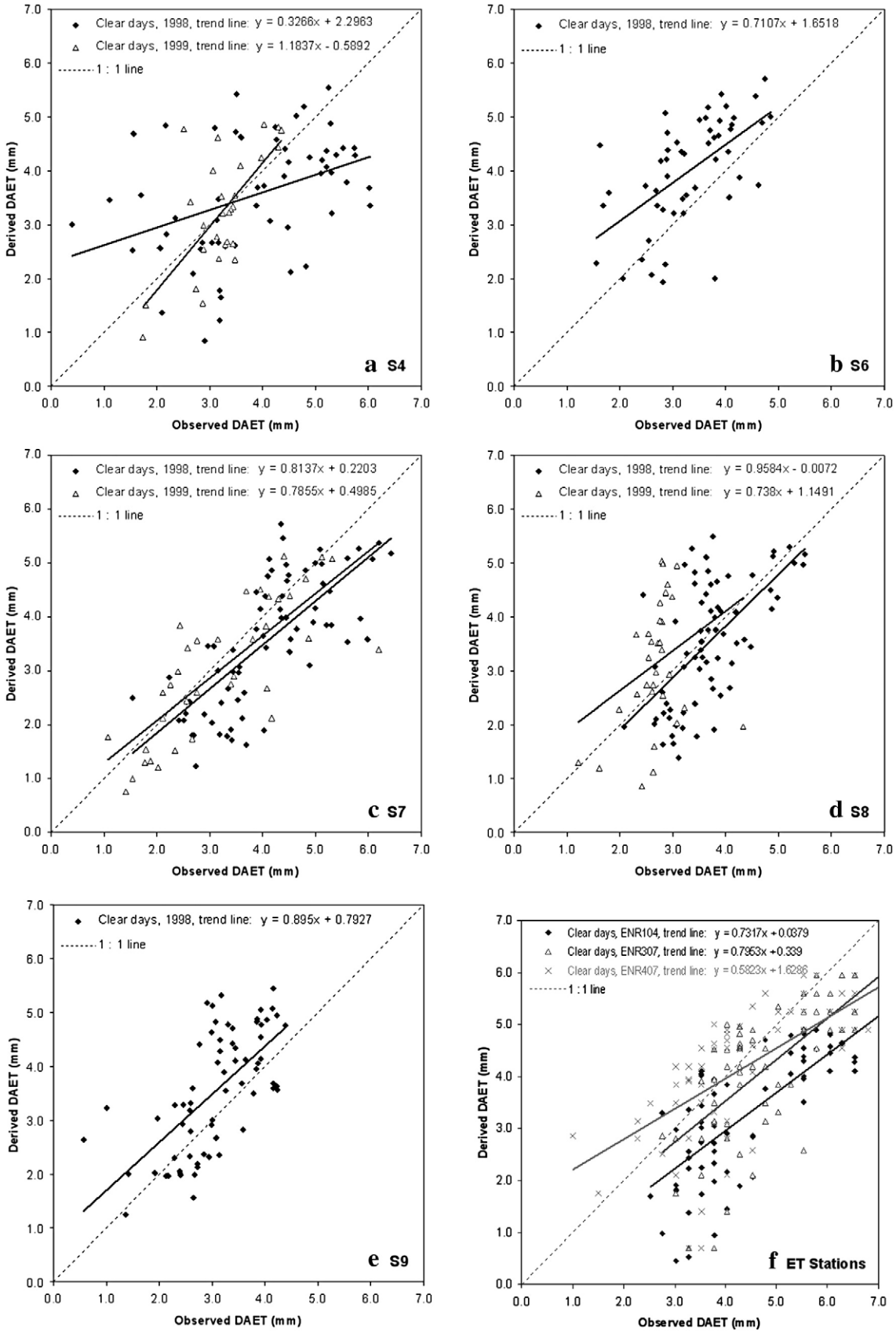

Fig. 8. (a through e) Comparison of derived *DAET* and observed *DAET* for most clear days at USGS stations (a through e) in 1998 and 1999, (f) Comparison of derived *DAET* and observed *DAET* at available *ET* stations for clear days in 1998. The data is not available for year 1999.

assumed to be representative or equivalent to the daily *EF*. Such an assumption may not always be valid since the daily overall cloud condition for a pixel may be very different from the snapshot at satellite overpass.

It is interesting to point out that the level of uncertainties depicted by two different types of metrics are comparable — one is the process variation itself depicted by the CV (e.g., the average $CV_{obs} = 12.7\%$), and the other is the relative estimation error depicted by $Bias/Mean_{obs}$ (e.g., 7.2%) or $RMSE/Mean_{obs}$ (22.4%) as shown in Table 2. When these two types of metrics are close in magnitudes, it may indicate that the estimation results have reached the accuracy limit of objectively quantifying the process.

4.4.2.2. Validation of EF for all days. To investigate the overall robustness of the SatDAET algorithm, we now compare satellite-based *EF* estimates for all days including both clear and cloudy days. The example shown in Fig. 7b is at S4 for all days in 1998 and 1999 when observation data are available. Except for a few points, the general patterns match those for clear day cases.

Table 3 gives a more comprehensive summary of statistical metrics for all available USGS stations. The average bias in *EF* for all days is −0.028 (Table 3) as compared to 0.049 for clear days (see Table 2). We have speculated in Section 2.2 that the error may be due to the underestimation of *EF* for cloudy pixels using extrapolated *EF* from clear pixels. The average RMSE for all days is 0.163 as compared to 0.158 for clear days. Although there are occasions when the algorithm has large biases, for example, 14.4% at S6 in 1998, it has a consistent performance overall for clear and cloudy days. Satellite VIS, NIR and IR channels can not provide reliable land surface information for partially cloudy and cloudy days as well as for off nadir observations, the spatial and temporal interpolation components in the SatDAET algorithm have shown the capability to reproduce the space–time structure of *EF* reasonably well for all days. Table 3 also implies that the results from interpolation for all days are not worse than those directly derived for clear days (Table 2).

4.4.3. Validation of DAET

4.4.3.1. Validation of DAET for clear days. We have compared derived *DAET* and observed *DAET* at available USGS stations and additional *ET* stations in 1998 and 1999. Fig. 8a–e shows the comparison of derived *DAET* and the observed *DAET* at USGS stations. We can see that in 1998 all stations except S4 have reasonably good results with low bias and RMSEs (as well as high correlation coefficients — see later in Table 4), while in 1999, results at S4 are much better than the previous year but results at S8 give worse correlation coefficient than the previous year. The number of days in comparison for 1998 and 1999 are different, with less days in 1999. The reason (among others) for the low correlation coefficient at S4 might be the inclusion of more "clear" days in 1998 but in fact some of these clear days are partly cloudy. We have compared the derived *DAET* and observed *DAET* at available *ET* stations operating in 1998 (Fig. 8f). There is a consistent underestimation of *DAET* while the correlation coefficients are relatively high (e.g., from 0.686 to 0.743).

Overall, Fig. 8 indicates that the SatDAET algorithm provides reasonably good estimates of *DAET* for a range of stations over the SFWMD domain for these 2 years. The bias and RMSE are low (while correlation coefficients are reasonably high). On average, bias is about −2.1% of observed mean, and RMSE 30.8% of observed mean). A consistent underestimation by the derived *DAET* for *ET* stations ENR104, ENR307, and ENR407 could be partly traced back to the effects discussed in Section 2.2 (i.e., underestimation of *EF* for cloudy pixels using *EF* detected for clear pixels), though it needs further examination, may also be due to the temporal smoothing used to derive daily *EF* and the underestimation of real R_n by the ground data interpolated R_n maps, and/or the possible over estimation of *ET* by the ground-based *ET* stations. In addition, scale discrepancy between the ground-based point observations and pixel scale satellite-based *DAET* estimates may explain a part of the error.

Table 4 is a summary of a comprehensive set of statistics for all available comparison stations in 1998 and 1999. The range of bias are moderately low — from −26.0% (of observed mean) to 20.1% (of observed mean) with an average of −2.1%, which is quite low. The RMSEs appear to be moderate to large ranging from 23.1% (of observed mean) to 45.0% with an average of 30.8%. The correlation coefficients are moderately high for most stations but low at S4 and S9 in 1998 and S8 in 1999 while RMSEs at these two stations also show the worst error magnitudes.

We notice that the coefficients of variation for the observed *DAET* are larger than those for *EF* in Table 2. On average, the coefficient of variation for observed series is 25.8% and that for estimated series is 33.8%. The reason for these is obviously due to the inclusion of ground-based R_n maps in obtaining *DAET* through Eq. (2), which appears to result in increased correlation coefficient while the level of relative errors indicated by relative bias and relative RMSE (in Table 4) are comparable to those in *EF* comparisons (in Table 2).

Even though a limited comparison is shown in this study, given the number of available ground stations, it is encouraging that the *DAET* estimation skills shown at most stations are superior and the overall average relative bias −2.1% and relative RMSE 30.8%.

4.4.4. Validation of DAET for all days

To investigate the robustness of the algorithm, SatDAET estimates, for all days including both clear and cloudy, were compared against the ground stations. Fig. 9 shows the comparison of *DAET* for USGS stations in 1998 and 1999. As expected, there is scattering in all the plots when cloudy days are included. Table 5 gives the summary of the comprehensive metrics set. Detailed inspections of these metrics as well as the scatter plots reveal that the major metrics are comparable to those for clear days.

Table 4
Summary statistics for clear days at USGS and *ET* stations that have *DAET* observations in 1998 and 1999.

Year	Station	$Mean_{obs}$ (mm)	STD_{obs} (mm)	CV_{obs}	$Mean_{est}$ (mm)	STD_{est} (mm)	CV_{est}	Bias (mm)	RMSE (mm)	*R*	$Bias/Mean_{obs}$	$RMSE/Mean_{obs}$
1998	S4	3.770	1.319	35.0%	3.437	1.141	33.2%	−0.333	1.359	0.424	−8.8%	36.0%
	S6	3.311	0.827	25.0%	4.005	1.012	25.3%	0.694	1.097	0.581	20.1%	33.1%
	S7	4.071	1.077	26.5%	3.533	1.199	34.0%	−0.538	0.995	0.731	−13.2%	24.4%
	S8	3.682	0.729	19.8%	3.522	1.139	32.3%	−0.160	0.907	0.614	−4.4%	24.6%
	S9	2.683	0.498	18.6%	3.129	1.189	38.0%	0.466	1.206	0.309	16.6%	45.0%
	ENR104	4.494	1.240	27.6%	3.326	1.221	36.7%	−1.168	1.460	0.743	−26.0%	32.5%
	ENR307	4.874	1.059	21.7%	4.215	1.228	29.1%	−0.659	1.126	0.686	−13.5%	23.1%
	ENR407	4.443	1.448	32.6%	4.215	1.228	29.1%	−0.227	1.095	0.686	−5.1%	24.6%
1999	S4	3.240	0.635	19.6%	3.246	1.094	33.7%	0.006	0.789	0.687	0.2%	24.3%
	S7	3.219	1.263	39.2%	3.027	1.277	42.2%	−0.192	0.858	0.777	−6.0%	26.7%
	S8	2.683	0.498	18.6%	3.129	1.189	38.0%	0.446	1.206	0.309	16.6%	45.0%
Mean		3.679	0.963	25.8%	3.526	1.174	33.8%	−0.151	1.100	0.595	−2.1%	30.8%

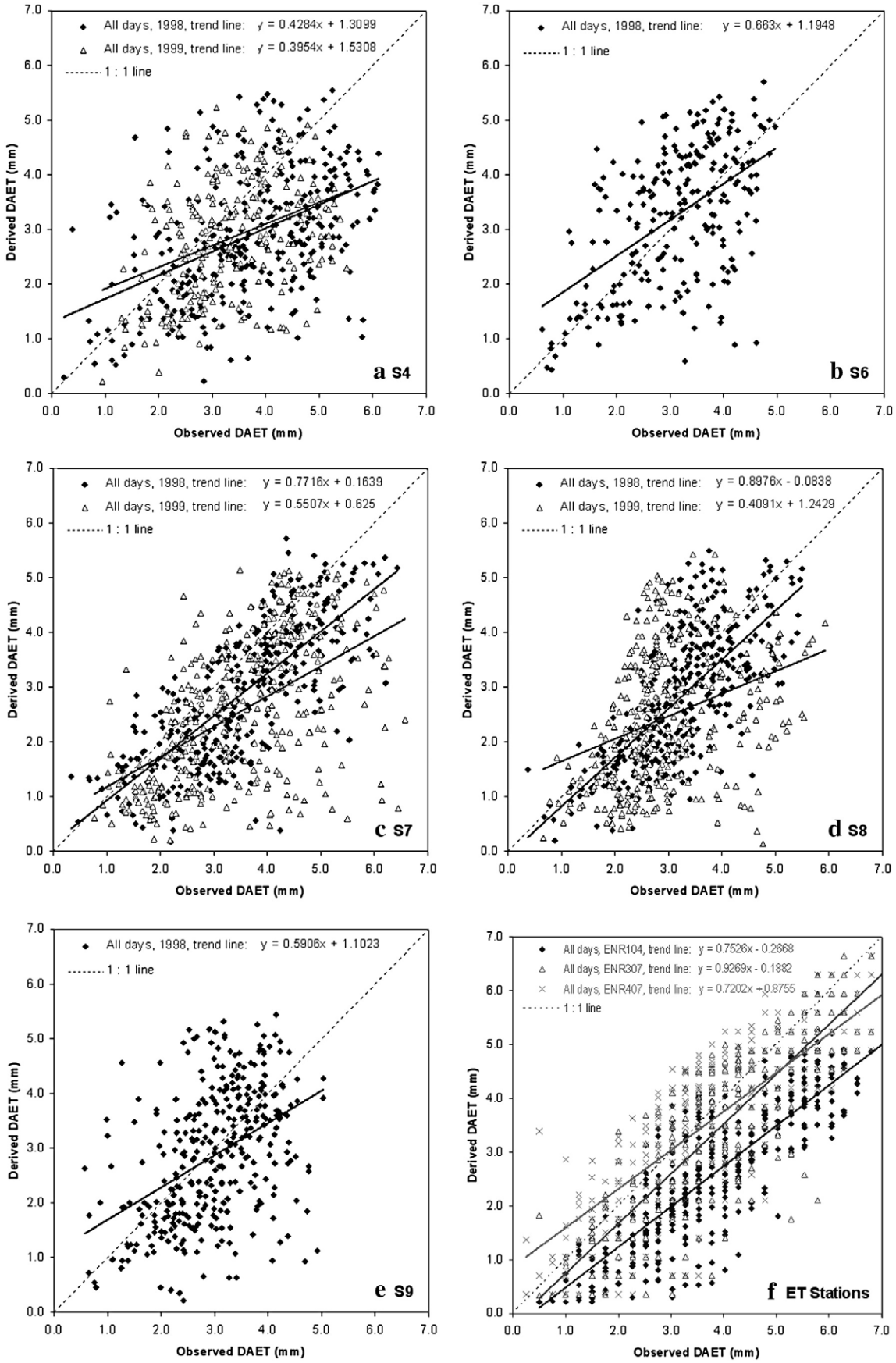

Fig. 9. (a through e) Comparison of derived *DAET* and observed *DAET* for all days at available USGS stations (a through e) in 1998 and 1999. (f) Comparison of derived *DAET* and observed *DAET* for all days at available *ET* stations in 1998.

Table 5
Summary statistics for all days at USGS and *ET* stations that have *DAET* observations in 1998 and 1999.

Year	Station	$Mean_{obs}$ (mm)	STD_{obs} (mm)	CV_{obs}	$Mean_{est}$ (mm)	STD_{est} (mm)	CV_{est}	Bias (mm)	RMSE (mm)	*R*	$Bias/Mean_{obs}$	$RMSE/Mean_{obs}$
1998	S4	3.694	1.256	34.0%	2.892	1.159	40.1%	−0.801	1.485	0.464	−21.7%	40.2%
	S6	3.098	1.006	32.5%	3.249	1.253	38.6%	0.151	1.122	0.532	4.9%	36.2%
	S7	3.515	1.227	34.9%	2.876	1.231	42.9%	−0.639	1.051	0.769	−18.2%	29.9%
	S8	3.262	0.954	29.2%	2.844	1.199	42.2%	−0.418	0.942	0.714	−12.8%	28.9%
	S9	2.989	0.890	29.8%	2.868	1.199	41.8%	−0.122	1.142	0.438	−4.1%	38.2%
	ENR104	3.845	1.396	36.3%	2.627	1.257	47.9%	−1.218	1.442	0.835	−31.7%	37.5%
	ENR307	4.068	1.412	34.7%	3.583	1.529	42.7%	−0.485	0.933	0.856	−11.9%	22.9%
	ENR407	3.789	1.746	46.1%	3.604	1.516	42.1%	−0.185	0.995	0.829	−4.9%	26.3%
1999	S4	3.355	0.988	29.4%	2.857	1.058	37.0%	−0.498	1.251	0.369	−14.8%	37.3%
	S7	3.451	1.249	36.2%	2.525	1.294	51.2%	−0.925	1.539	0.532	−26.8%	44.6%
	S8	2.958	0.989	33.4%	2.453	.1.235	50.3%	−0.505	1.397	0.328	−17.1%	47.3%
Mean		3.457	1.192	34.2%	2.943	1.270	43.3%	−0.513	1.209	0.606	−14.5%	35.4%

For year 1998, the performance at S4, S7 and S8 is not as satisfactory as those for clear days in terms of relative biases (i.e., −21.7%, −18.2% and −12.8% in Table 5 as compared to −8.8%, −13.2% and −4.4% in Table 4), while at S6 and S9, relative biases reduce from 20.1% and 16.6% (in Table 4) to 4.9% and −4.1% (in Table 5) respectively. For year 1999, at S4 and S7 relative biases increase from 0.2% and −6.0% (in Table 4) to −14.8% and −26.8% (in Table 5), while results are comparable (to those of clear days) for S8 in absolute magnitude of relative bias. The relative RMSEs increase mostly given the increased scattering seen from those scatter plots in Fig. 9 (a through e).

Fig. 9f provided comparison for all days at three *ET* stations in 1998. Overall, there is relatively small but consistent underestimation of *ET*. (The results are reasonably good with respect to high correlation coefficients). For ENR407, there are a few days with observed *DAET* equal to zero. These days are excluded from the model validation. It appears in Table 5 that the SatDAET algorithm performed better on *DAET* for *ET* stations compared to USGS stations in terms of correlation coefficient and relative RMSE, which is encouraging since the R_n for these *ET* stations are estimated from ground-based interpolation unlike those directly observed at the USGS stations. On average, when all USGS and *ET* stations are considered, the correlation coefficient is 0.606, relative bias is −14.5% and relative RMSE amounts to 35.4%. Further, we found the statistical metrics for derived *DAET* at ENR307 (e.g., Bias = −0.485 mm, RMSE = 0.933 mm, and $R = 0.856$, see Table 5) is comparable to the within pixel variation of *DAET* (see Section 4.2) where observed *DAET* at ENR407 is compared to that at ENR307 (e.g., Bias = −0.310 mm, RMSE = 0.844 mm, and $R = 0.903$).

EF at USGS stations indicate that the stations are very "wet" since *EF* values are relatively large. Observed *EF* values for USGS stations are clustered at the upper-right corner of the scatter plots in Fig. 7a and b (with *EF* axes scaled between $EF = 0.0$ to $EF = 1.0$) indicating that the observed *EF* values have a small range of variation at USGS stations. Our algorithm reproduced the small range of observed *EF* values with relatively high accuracy in terms of relative bias and relative RMSE though correlation coefficients are low. Our estimation of *EF* relies only on satellite-based data with no site specific tuning of parameters. These results suggest that our satellite remote sensing based *EF* algorithm has reached its accuracy limit within an acceptable error range.

For *DAET* estimation assessment, it is shown that *DAET* values have a larger range of variation than those of *EF* for USGS stations. This is indicated by comparison of coefficients of variation for the observed series of *EF* and *DAET*. The increased correlation coefficients and the relative error range still imply that by utilizing additional R_n data (which in this case is derived from ground-based stations) the SatDAET algorithm is capable of monitoring *DAET* that has a larger variation range.

Further, we have compared the annual mean of domain (i.e., map) averaged *DAET* from the SatDAET algorithm with the annual mean of averaged *DAET* from all ground-based stations, it is very encouraging to observe that the SatDAET algorithm has 14% difference for 1998 and 19% difference for 1999 (both underestimations) comparing to those observation derived quantities. Such levels of error are comparable to the bounds of instrumental accuracy and observational methods.

5. Discussion and conclusion

The objective of the current study was to develop and validate a robust and reliable daily *ET* estimation model for all sky (comprising of cloudy and clear sky) conditions using remote sensing data. Our proposed SatDAET algorithm first estimates the Evaporative Fraction (*EF*) by utilizing the relationship between *NDVI* and radiometric surface temperature observed from AVHRR for each day. Then spatio-temporal interpolation and filtering techniques are applied to obtain daily *EF* values for cloudy pixels and to produce continuous *EF* maps for the entire region. Daily Actual *ET* (*DAET*) maps are derived from *EF* maps and net radiation data obtained from ground-based observations. Comparisons between satellite derived *DAET* and ground measured *DAET* showed overall low bias and RMSE (as well as moderately high correlation coefficient) for both clear and cloudy days in 1998 and 1999.

The proposed SatDAET algorithm, primarily driven by satellite data, appears to be robust and can produce near real-time *DAET* monitoring over large heterogeneous areas at a fine space and time resolution. We argue that the strength of the proposed *ET* estimates should be evaluated not only by how closely they reproduce surface based point observations but also by their ability to provide a spatially consistent and distributed *ET* map over a large heterogeneous domain. The improvement in space–time estimates of *ET* at 1 km scale over the heterogeneous SFWMD domain, despite its shortcomings, is substantial compared to currently available spatially distributed *ET* estimates and the cost of maintaining surface based observation network.

The SatDAET algorithm looks at the instantaneous surface thermal dynamic balance reflected in the *T*–VI space, thus the contextual information of the spatial distribution of the (more dynamic) temperature variation over the (less dynamic) vegetation variations, to obtain *DAET* over large areas. On a given day over a specific region, contextual spatial information about surface temperature variability among nearby pixels is not likely to change significantly. Such contextual information provides the basis of using instantaneous *T*–VI diagrams to derive *EF* (Venturini et al., 2004) It is worthwhile to note that *EF* maps derived from multiple sensor systems (with different observation times) have a small range of variations while other parameters such as *NDVI* and *T* derived from multiple sensors are likely to have large range of variations. The SatDAET approach allows us to look at the relative values of radiometric surface temperature rather than an exact land surface temperature thereby minimizing the impact of errors associated with estimation of surface temperature from satellite. This is achieved by the interpolation of *EF*

value for a certain image pixel within the trapezoidal (or triangular) *T*–VI space based on the position of the pixel's *T* relative to the lower bound (i.e., base) and upper bound (i.e., warm edge) of the trapezoid space, while such bounds are also determined within the same remote sensing information context. The bounds of the triangular (trapezoidal) *T*–VI diagram were defined by a warm edge, open water temperature, and *NDVI*s for bare soil and full vegetation covers. Our findings indicate that it is effective to use remotely sensed average inland water surface radiometric temperature as the lower base of the trapezoid space (Islam et al., 2002). Such temperature is normally lower than radiometric surface temperature over dense vegetation cover at daytime. As a result, *EF* derived for dense vegetation cover is normally less than 1.0 for all cases. We note here that *no other surface or atmospheric measurements are required to estimate EF for all the pixels over a given region.*

In other studies over a different region, we have demonstrated that the methodology can capture the spatial and temporal variability of ϕ satisfactorily (e.g. Jiang and Islam, 1999, 2001, 2003). For a particular site, use of a constant value for *EF* rather than that from the satellite-based method may result in a good match between estimation and observations. Such a treatment, however, will lose generality since most field experiment data show distinct seasonality for *EF*.

It is partly true that the good correlations between measured and estimated *DAET* were a result of using same net radiation at the validation sites. Since *EF* is a fractional coefficient applied to net radiation to obtain *DAET* (e.g. Eq. (2) shows *DAET* is linearly related to *EF*), our results suggest that the remote sensing derived *EF* does not have large estimation error. In practice, when neither net radiation nor *EF* is known, the implications from different comparison studies may be more complicated or even misleading. An advantage of our approach is that *EF* or ϕ can be independently derived from remote sensing data without directly referring to other surface fluxes terms (e.g. R_n, *G*, etc.).

We have eliminated the requirement for site specific tuning of model parameters which makes the proposed SatDAET algorithm more practical for operational purposes. We acknowledge that some water bodies like Lake Okeeechobee did show as a discrete feature due to spatial interpolation of R_n. We plan to expand the current algorithm for estimation of *DAET* over heterogeneous areas using a more sophisticated method in which daily radiation (based on our recent work by Bisht et al., 2005) will be estimated from remote sensing thus the whole SatDAET algorithm will be completely dependent on satellite-based estimation, eliminating the need for ground-based data.

The source of error for SatDAET algorithm, though not discussed comprehensively in this study, is primarily the cloud contamination and other factors that affect the multi-channel remote sensing image quality for a given region based on the experience gained through practical implementation of this approach using a large volume of remote sensing data. The simplified (i.e., linear) treatment of distribution of the ϕ parameter within the triangular (or trapezoid) *T*–VI space and the non-explicit inclusion of other information and processes (such as surface humidity and wind speed) could be other sources of uncertainty intrinsic to the primarily satellite-based approach. Considering the trade-off between sophisticated modeling approach and the realistic constraints and expense in obtaining required model data for heterogeneous domain, we conclude that the SatDAET algorithm is a simple and easily applicable approach to assist practical near real-time water resources management needs.

Acknowledgements

This work was supported by a contract from the South Florida Water Management District and accomplished through collaboration among SFWMD, University of Cincinnati, Tufts University, MIT, NOAA/NESDIS/ORA and I. M. Systems Group, Inc. Part of this work was also supported by a grant from the National Research Institute Competitive Grants Program of the United States of America (MASR 2004-00888). Comments on technical implementation from SFWMD, and from USGS scientist Dr. Sumner to refine the algorithm components, and comments on improving the manuscript from Dr. Arnold Gruber of NOAA/NESDIS Cooperative Institute for Climate Studies are gratefully acknowledged.

References

Bastiaanssen, W.G., Pelgrum, H., Menenti, M., Feddes, R.A., 1996. Estimation of surface resistance and Priestley–Taylor — parameter at different scales. In: Stewart, J., Engman, E., Feddes, R., Kerr, Y. (Eds.), Scaling up in Hydrology Using Remote Sensing.

Batra, N., Islam, S., Venturini, V., Bisht, G., Jiang, L., 2006. Estimation and comparison of evapotranspiration from MODIS and AVHRR sensors for clear sky days over the Southern Great Plains. Remote Sens. Environ. 103, 1–15.

Betts, A.K., Hall, J.H., 1998. FIFE surface climate and site-average dataset 1987–89. J. Atmos. Sci. 55 (7), 1091–1108.

Bisht, G., Venturini, V., Jiang, L., Islam, S., 2005. Estimation of net radiation using MODIS (Moderate Resolution Imaging Spectroradiometer) terra data for clear sky days. Remote Sens. Environ. 97, 52–67.

Bras, R., 1990. Hydrology: An Introduction to Hydrologic Science. Addison-Wesley, p. 642.

Carlson, T.N., Gillies, R.R., Schmugge, T.J., 1995. An interpretation of methodologies for indirect measurement of soil water content. Agric. For. Meteorol. 77, 191–205.

Carlson, T.N., Ripley, D.A.J., 1997. On the Relationship Between NDVI, Fractional Vegetation Cover and Leaf Area Index. Remote Sensing Environment 62, 241–252 (2004).

German, E.R., 2000. Regional evaluation of evapotranspiration in the everglades. USGS Water Resources Investigation Report 00-4217, Tallahassee, Florida.

Hall, F.G., Townshend, J.R., Engman, E.T., 1995. Status of remote sensing algorithms for estimation of land surface state parameters. Remote Sens. Environ. 41, 138–158.

Islam, S., Eltahir, E., Jiang, L., 2002. Satellite-based evapotranspiration estimates. Final Project Report Submitted to South Florida Water Management District, p. 74.

Jiang, L., Islam, S., 1999. A methodology for estimation of surface evapotranspiration overlarge areas using remote sensing observations. Geophys. Res. Lett. 26 (17), 2773–2776.

Jiang, L., Islam, S., 2001. Estimation of surface evaporation map over Southern Great Plains using remote sensing data. Water Resour. Res. 37 (2), 329–340.

Jiang, L., Islam, S., 2003. An intercomparison of regional latent heat flux estimation using remote sensing data. Int. J. Remote Sens. 24 (11), 2221–2236.

Kitanidis, P., 1997. Introduction to Geostatistics: Applications in Hydrogeology. Cambridge University Press. 271 pp.

Kogan, F.N., 1990. Remote sensing of weather impacts on vegetation in nonhomogeneous areas. Int. J. Remote Sens. 11, 1405–1419.

Kustas, W.P., Perry, E.M., Doraiswamy, P.C., Moran, M.S., 1994. Using satellite remote sensing to extrapolate evapotranspiration estimates in time and space over a semiarid rangeland basin. Remote Sens. Environ. 49, 275–286.

Priestley, C.H.B., Taylor, R.J., 1972. On the assessment of surface heat flux and evaporation using large-scale parameters. Mon. Weather Rev. 100, 81–92.

Shuttleworth, W.J., 1991. Evaporation models in hydrology. In: Schmugge, T.J., Andre, J.-C. (Eds.), Land Surface Evaporation: Measurement and Parameterization. Springer-Verlag, New York, pp. 93–120.

Singh, V.P., 1988. Hydrological Systems, vol. 2. Prentice Hall Publication, NJ, USA.

Van Dijk, A., Callis, S.L., Sakamoto, C.M., Decker, W.L., 1987. Smoothing vegetation index profiles: an alternative method for reducing radiometric disturbance in NOAA/AVHRR data. Photogramm. Eng. Remote Sensing 53, 1059–1067.

Venturini, V., Bisht, G., Islam, S., Jiang, L., 2004. Comparison of evaporative fractions estimated from AVHRR and MODIS sensors over South Florida. Remote Sens. Environ. 93, 77–86.

Willmott, C.J., 1982. Some comments on the evaluation of model performance. Bull. Am. Meteorol. Soc. 63 (11), 1309–1313.

Willmott, C.J., Wicks, D.E., 1980. An empirical method for the spatial interpolation of monthly precipitation within California. Phys. Geogr. 1, 59–73.